Causes of the El Niño and La Niña Amplitude Asymmetry in the Equatorial Eastern Pacific

JINGZHI SU,* RENHE ZHANG,+ TIM LI,# XINYAO RONG,+ J.-S. KUG,# AND CHI-CHERNG HONG@

* *Chinese Academy of Meteorological Sciences, and Nansen-Zhu International Research Centre, Institute of Atmospheric Physics, Chinese Academy of Sciences, Beijing, China*
+ *Chinese Academy of Meteorological Sciences, Beijing, China*
# *Korea Ocean Research and Development Institute, Ansan, South Korea*
@ *Department of Science Education, Taipei Municipal University of Education, Taiwan*

(Manuscript received 16 October 2008, in final form 6 March 2009)

ABSTRACT

The amplitude asymmetry between El Niño and La Niña is investigated by diagnosing the mixed-layer heat budget during the ENSO developing phase by using the three ocean assimilation products: Simple Ocean Data Assimilation (SODA) 2.0.2, SODA 1.4.2, and the Global Ocean Data Assimilation System (GODAS). It is found that the nonlinear zonal and meridional ocean temperature advections are essential to cause the asymmetry in the far eastern Pacific, whereas the vertical nonlinear advection has the opposite effect. The zonal current anomaly is dominated by the geostrophic current in association with the thermocline depth variation. The meridional current anomaly is primarily attributed to the Ekman current driven by wind stress forcing. The resulting induced anomalous horizontal currents lead to warm nonlinear advection during both El Niño and La Niña episodes and thus strengthen (weaken) the El Niño (La Niña) amplitude. The convergence (divergence) of the anomalous geostrophic mixed-layer currents during El Niño (La Niña) results in anomalous downwelling (upwelling) in the far eastern equatorial Pacific, which leads to a cold nonlinear vertical advection in both warm and cold episodes.

1. Introduction

El Niño–Southern Oscillation (ENSO) is the dominant interannual variability in the tropical Pacific. A considerable number of observational, theoretical, and modeling studies have contributed over the past decades to the understanding of the structures and basic mechanisms of the ENSO cycle (e.g., Rasmusson and Carpenter 1982; Cane and Zebiak 1985; Philander 1990; Zhang and Chao 1993a). There are several theories for the ENSO oscillations: for example, the delayed oscillator (Battisti and Hirst 1989; Suarez and Schopf 1988), the self-excited oscillations in the nonlinear tropical air–sea coupled system (Zhang and Chao 1993b), the recharge–discharge or stationary SST mode (Jin 1997; Li 1997), the western Pacific oscillator (Weisberg and Wang 1997a,b), and the advective–reflective oscillator (Picaut et al. 1997).

However, a remaining open question is what causes the ENSO amplitude asymmetry. Observations show that the amplitude of sea surface temperature anomalies (SSTAs) in the eastern equatorial Pacific is significantly larger during El Niño episodes than during La Niña episodes (Burgers and Stephenson 1999). This asymmetric aspect of ENSO cannot be explained by the conceptual model mentioned earlier, in which ENSO is portrayed as a regular and periodic oscillation. An and Jin (2004, hereafter AJ04) showed that nonlinear dynamical thermal advections could play important roles in the amplitude asymmetry between El Niño and La Niña. The asymmetric atmospheric response to equal-strength but opposite SST anomalies is another possible cause (Hoerling et al. 1997; Kang and Kug 2002). The oceanic tropical instability waves in the eastern equatorial Pacific tend to be more active during La Niña than El Niño (Vialard et al. 2001), which may also favor the ENSO amplitude asymmetry.

To reveal specific processes that give rise to the ENSO amplitude asymmetry, Jin et al. (2003) and AJ04 analyzed three-dimensional (3D) temperature advection terms and found that nonlinear vertical temperature advections

Corresponding author address: Dr. Renhe Zhang, Chinese Academy of Meteorological Sciences, No. 46 Zhong-Guan-Cun South Avenue, Haidian district, Beijing 100081, China.
E-mail: renhe@cams.cma.gov.cn

DOI: 10.1175/2009JCLI2894.1

make a major contribution. Because the sign of the nonlinear advection term is determined by the phase relationship between the anomalous temperature and velocity, the final results depend crucially on the quality of the simulated ocean current and temperature fields used in the heat budget diagnosis. The analyses of Jin et al. (2003) and AJ04 were mainly based on an older version of the National Centers for Environmental Prediction (NCEP) Ocean Data Assimilation System (ODAS) and the Simple Ocean Data Assimilation (SODA) beta 7 version. Over recent years, the ODAS has been updated by the new version of the Global Ocean Data Assimilation System (GODAS), and several updated versions of SODA have also been released.

Several issues related to the nonlinear temperature advection need be addressed. For example, do the nonlinear temperature advections keep the same sign from the El Niño developing phase to its decaying phase? What is the difference between horizontal and vertical advections? What determines anomalous horizontal and vertical currents in the far eastern equatorial Pacific? The release of the newly updated ocean assimilation systems motivates us to revisit the mechanism of ENSO amplitude asymmetry. This paper attempts to address those questions based on the ocean fields derived from the GODAS and the new version SODA products.

The rest of this paper is organized as follows: section 2 describes the data and method. Section 3 shows the temperature skewness. An analysis of the mixed-layer heat budget is given in section 4. The processes that cause the anomalous zonal and meridional currents are discussed in section 5. Finally, conclusions and discussion are presented in the last section.

2. Data and methods

The primary data used in this study are the SODA reanalysis version 2.0.2 (Carton and Giese 2008). The ocean model in the data assimilation is based on the Parallel Ocean Program (Dukowicz and Smith 1994) with a horizontal resolution of 0.4° longitude by 0.25° latitude. There are 40 levels in the vertical, with a resolution of about 10 m in the upper 100 m. For this study, all the monthly mean oceanic variables are interpolated into a horizontal resolution of 0.5° × 0.5°. Forced by daily wind stresses and heat fluxes from the 40-yr European Centre for Medium-Range Weather Forecasts Re-analysis, SODA 2.0.2 assimilates all the available hydrographic data, including expendable bathythermograph (XBT) from 1958 to 2000.

To reduce the uncertainty in the mixed-layer heat budget and ocean currents, SODA 1.4.2 (Carton and Giese 2008) and the GODAS (Saha et al. 2006) products are also used. Different from SODA 2.0.2, SODA 1.4.2 is forced by NCEP wind stress, whereas the SST is restored toward the observations. Although the vertical velocity field is a direct output variable in version 2.0.2, it is diagnosed from the horizontal currents based on the continuity equation in version 1.4.2. GODAS is based on a quasi-global configuration of the Geophysical Fluid Dynamics Laboratory Modular Ocean Model (MOM) version 3. The model domain extends from 75°S to 65°N, and it has a constant zonal resolution of 1° and a variable meridional grid that ranges from a resolution of 1/3° at the equator to 1° at 10° and 1° poleward. The model has 40 levels with a 10-m resolution in the upper 200 m. Forced by the momentum flux, heat flux, and freshwater flux from the NCEP-2 atmospheric reanalysis, the GODAS assimilates temperature profiles from XBTs, tropical atmosphere–ocean moorings, and Argo profiling floats.

The skewness is used to quantify the deviations from normality. It measures the asymmetry of a probability distribution function, with a value of 0 representing a normal distribution (White 1980). The skewness is defined as Skewness $= m_3/(m_2)^{3/2}$, where m_k is the kth moment, $m_k = 1/N \sum_{i=1}^{N}(x_i - \overline{X})^k$; x_i is the ith observation (seasonal mean field in here); $\overline{X}$ is the long-term climatological mean; and N is the number of observations. The statistical significance of the skewness may be estimated based on the number of independent samples (White 1980). Because the time series of SSTA might not be statistically independent, we use a range estimate instead, following Hong et al. (2008a). It is estimated that, for a given sample length, a confidence level of 95% corresponds to the amplitude of the skewness exceeding ±0.67.

To understand the relative roles of ocean advection and surface heat flux terms in causing the asymmetric SSTA tendencies, the oceanic mixed-layer heat budget is diagnosed. The mixed-layer temperature (MLT) tendency equation may be written as

$$\frac{\partial T'}{\partial t} = -(\mathbf{V}' \cdot \nabla \overline{T} + \overline{\mathbf{V}} \cdot \nabla T') - (\mathbf{V}' \cdot \nabla T') + \frac{Q'_{\text{net}}}{\rho C_P H} + R, \tag{1}$$

where $\mathbf{V} = (u, v, w)$ represents the 3D ocean current, $\nabla = (\partial/\partial x, \partial/\partial y, \partial/\partial z)$ denotes the 3D gradient operator, $(')$ represents the anomaly variables, $(\overline{\ })$ represents the climatological annual cycle variables, $-(\mathbf{V}' \cdot \nabla \overline{T} + \overline{\mathbf{V}} \cdot \nabla T')$ is the sum of linear advection terms, $-(\mathbf{V}' \cdot \nabla T')$ denotes 3D nonlinear temperature advection terms, Q_{net} represents the net heat flux at the ocean surface, R represents the residual term, $\rho = 10^3$ kg m^{-3} is the density of water, $C_P = 4000$ J kg^{-1} K^{-1} is the specific heat of water, and $H = 30$ m denotes the climatological mixed-layer depth. All of the mixed-layer fields are

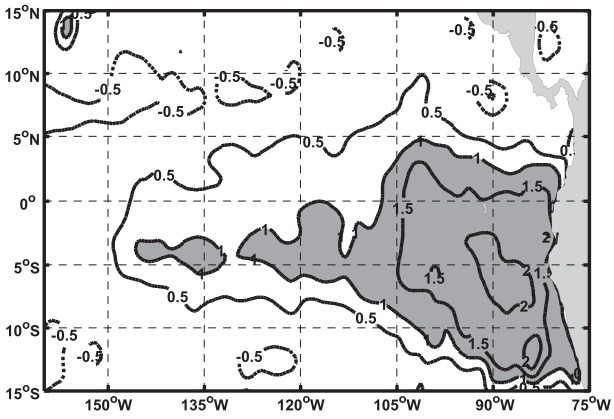

FIG. 1. Skewness of DJF SST anomalies. Contour interval is 0.5. Contours with values above 1.0 are shaded.

calculated based on their depth average. The climatological annual cycle is calculated based on the period of 1958–2000 for SODA and 1980–2000 for GODAS. The heat budget analysis is performed for both El Niño and La Niña composites, following the methodology used in Li et al. (2002) and Hong et al. (2008a,b).

3. Temperature skewness

The amplitude asymmetry of El Niño and La Niña episodes may be quantitatively represented by the skewness of the SSTA (Fig. 1). Note that the positive skewness is confined in the eastern equatorial Pacific. The skewness is most significant near the South American coast between 5°N and 10°S. The skewness magnitude decreases gradually toward the west. Because the significant temperature skewness is primarily located east of 110°W, in the following our budget analysis is focused on the region (5°N–5S°, 110°–80°W; called EP110). The maximum skewness in EP110 occurs during the boreal winter.

A heat budget analysis is performed for each individual El Niño and La Niña case. As shown in Fig. 2, the developing phase of a warm (cold) case begins at a time when the positive (negative) temperature anomaly in EP110 occurs and ends at the mature phase, when the temperature anomaly tendency is zero. Before selecting the developing phase, the time series of the temperature anomaly is smoothed with a 7-month running mean to remove the high-frequency signals. The developing periods for seven El Niño years are as follows: March–September 1965, February–September 1972, February–October 1976, February 1982–January 1983, June 1986–June 1987, January 1990–December 1991, and January–November 1997. The developing periods for seven La Niña years are as follows: January–October 1964, February 1966–September 1967, February–November 1970, April–October 1973, January 1984–April 1985, January–September 1988, and October 1998–October 1999. An alternative way to define the developing phase is based on the composite ENSO evolution. As the mature phase of the composite ENSO occurs in December–February (DJF), one may analyze the SST tendency averaged during June–November. It turns out that the heat budget analyses derived from both the methods are quite similar.

An examination of composite SSTA evolutions during El Niño and La Niña reveals that the SSTA tendency differs significantly between the warm and cold episodes during their developing phase. The temperature tendency during the developing phase in EP110 is 0.18° and -0.10°C month^{-1} in El Niño and La Niña composites, respectively (Fig. 3). Given that the ratio of MLT at EP110 between El Niño and La Niña in their mature phase is also about 3:2, it is obvious that the temperature tendency difference in the developing phase is responsible for the El Niño and La Niña amplitude asymmetry in the mature phase. In the following, we focus on analyzing the cause of the asymmetry of the MLT tendency during the developing phase of El Niño and La Niña.

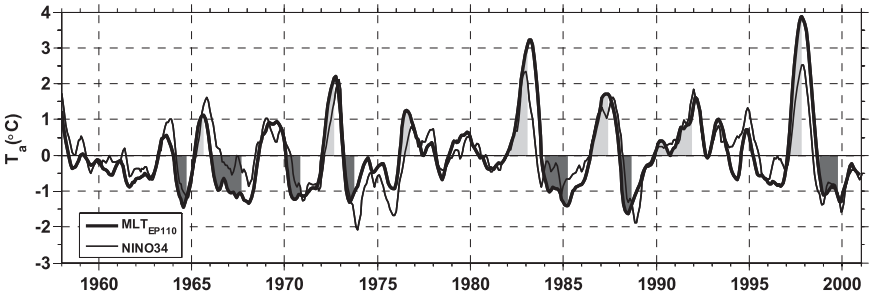

FIG. 2. The time series of mixed-layer temperature anomalies of region EP110 (5°N–5°S, 110°–80°W). The developing phases for El Niño (La Niña) cases are indicated by the gray (black) shading. The time series is smoothed with a 7-month running mean. The time series of 3-month mean observed SST anomalies of Niño-3.4 is also plotted as a light line.

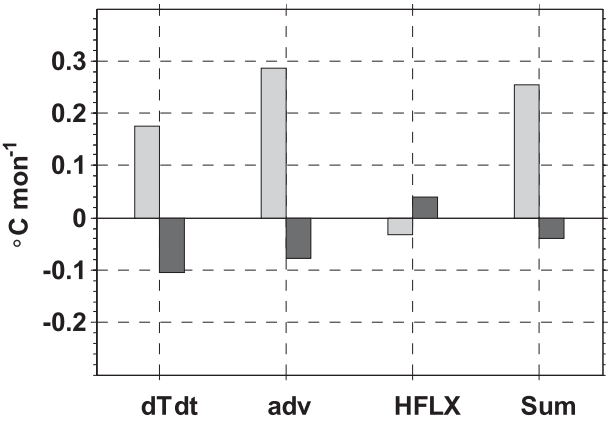

FIG. 3. The mixed-layer temperature tendency terms (left)–(right) along the *x* axis: the observed temperature tendency, the 3D temperature advection, the surface flux heating, and the sum of the advection and the surface heat flux. The calculation is based on SODA 2.0.2. Gray and black bars represent composite results for El Niño and La Niña events, respectively. All the terms are averaged over the far eastern equatorial Pacific (5°N–5°S, 110°–80°W) for the developing phases.

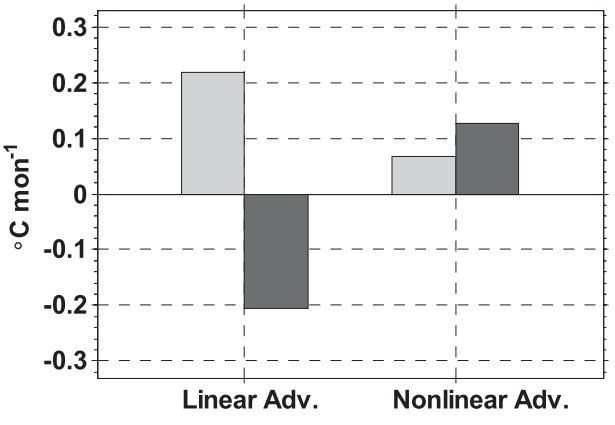

FIG. 4. As in Fig. 3, but for the linear and nonlinear temperature advection terms for El Niño and La Niña composites.

4. A mixed-layer heat budget analysis

The heat budget analysis indicates that the asymmetry of the MLT tendency in EP110 between the El Niño and La Niña episodes is primarily attributed to the 3D ocean temperature advection (Fig. 3). The net surface heat flux terms actually tend to reduce the tendency contrast between the warm and cold episodes and thus have no contribution to the amplitude asymmetry. Although the heat budget is not exactly in balance because of the uncertainty of surface heat fluxes and oceanic subgrid processes, the asymmetry in the MLT tendency is adequately demonstrated and is consistent with the observed; that is, the amplitude of the positive MLT tendency during El Niño is much greater than its La Niña counterpart.

The 3D ocean temperature advection can be further decomposed into linear and nonlinear advection terms (by separating the climatological annual cycle and interannual anomaly fields). The sum of the linear and nonlinear advection terms in contributing to the asymmetric MLT tendency is shown in Fig. 4. The linear advection terms are 0.22° and −0.21°C month^{-1} in El Niño and La Niña episodes respectively. This indicates that the linear advection terms primarily contribute to the growth of El Niño and La Niña. The nonlinear advection terms, on the other hand, are positive in both El Niño (0.07°C month^{-1}) and La Niña (0.13°C month^{-1}) episodes. This means that the nonlinear advections tend to enhance the warm events but weaken the cold events and thus are responsible for the amplitude asymmetry.

The nonlinear advection terms can be further decomposed into the zonal, meridional, and vertical advection terms (Fig. 5a). The zonal nonlinear advection terms tend to warm the MLT in both the El Niño (0.03°C month^{-1}) and La Niña (0.12°C month^{-1}) composites. The meridional nonlinear advection terms are also positive for both warm and cold episodes (0.11°C month^{-1} in El Niño and 0.07°C month^{-1} in La Niña). Thus, both the zonal and meridional nonlinear advections favor the positive skewness in the far eastern equatorial Pacific. The vertical nonlinear advection terms, on the other hand, tend to cool the MLT in both El Niño (−0.07°C month^{-1}) and La Niña (−0.06°C month^{-1}) events.

To examine how the result above is sensitive to different data products, we carried out the same budget analysis using the SODA 1.4.2 and GODAS data. Because the GODAS outputs begin from 1980, only the years after 1980 are used for calculating the El Niño and La Niña composites. As in SODA 2.0.2, the linear advection terms in SODA 1.4.2 also favor the growth of both El Niño and La Niña episodes, with an amplitude of about 0.2°C month^{-1} (not shown). The nonlinear advection terms show an asymmetric feature, being positive in both El Niño and La Niña episodes (Fig. 5b). Although differing in amplitude, the relative contributions of the zonal, meridional, and vertical advection terms in SODA 1.4.2 are the same as those in SODA 2.0.2 (Fig. 5). A similar conclusion may be derived from the GODAS data. Thus, the results based on SODA 1.4.2 and GODAS confirm the conclusion that the positive skewness is caused by the nonlinear horizontal advection.

Figure 6 illustrates the horizontal distribution of the nonlinear advection terms. Note that both the positive horizontal nonlinear advection and the negative vertical nonlinear advection fields are primarily confined in the far eastern equatorial Pacific.

How do the nonlinear horizontal advection terms contribute to the positive skewness in the far eastern

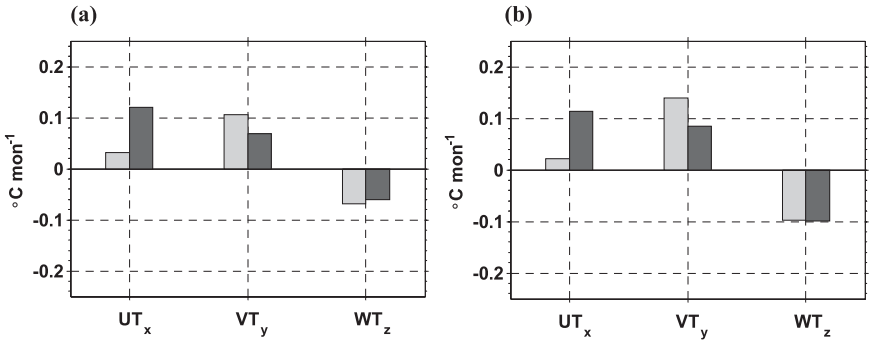

FIG. 5. (a) As in Fig. 3, but for the zonal, meridional, and vertical components of nonlinear advection terms. (b) As in (a), but based on SODA 1.4.2.

Pacific? To address this question, we first examine the anomalous ocean temperature and current fields along the equator (Figs. 7a,b). For the El Niño composite, the zonal current anomalies in the mixed layer are eastward ($u' > 0$), with the maximum temperature anomaly being located around 105°W. East of 105°W, the negative zonal temperature gradient ($\partial T'/\partial x < 0$) and the positive current anomalies lead to a warm zonal nonlinear advection ($-u'\partial T'/\partial x > 0$). For the La Niña composite, the minimum MLT anomaly resides around 110°W. The anomalous westward current ($u' < 0$) leads to a positive zonal nonlinear advection ($-u'\partial T'/\partial x > 0$) east of 110°W. Therefore, positive zonal nonlinear advections appear in both El Niño and La Niña composites.

From the meridional–vertical section (Figs. 7c,d), it is seen that the maximum MLT anomaly is located south of the equator (about 1°S) during El Niño. Thus, the meridional temperature gradient is negative at the equator,

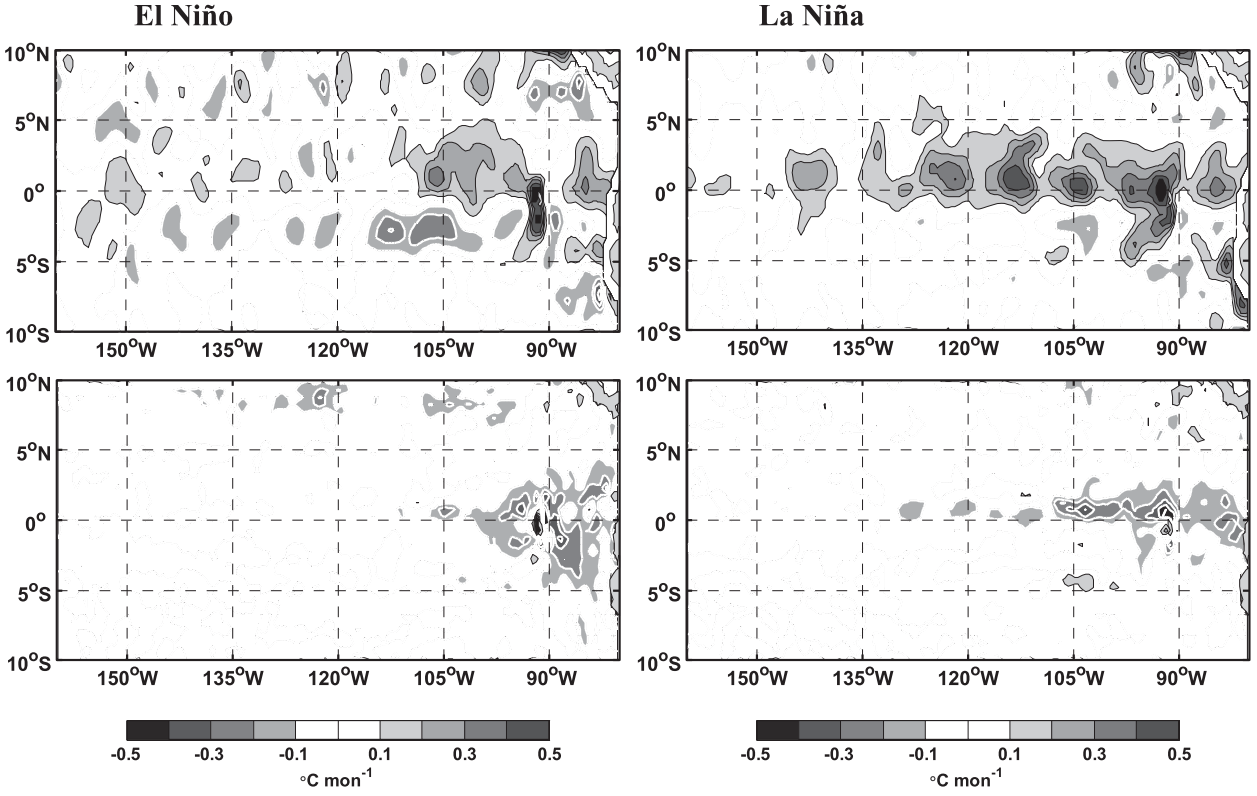

FIG. 6. Composite (top) horizontal and (bottom) vertical nonlinear temperature advection fields during the developing phases of (left) El Niño and (right) La Niña from SODA 2.0.2. The shadings with black (white) contours indicate positive (negative) values with absolute values >0.1°C month^{-1}.

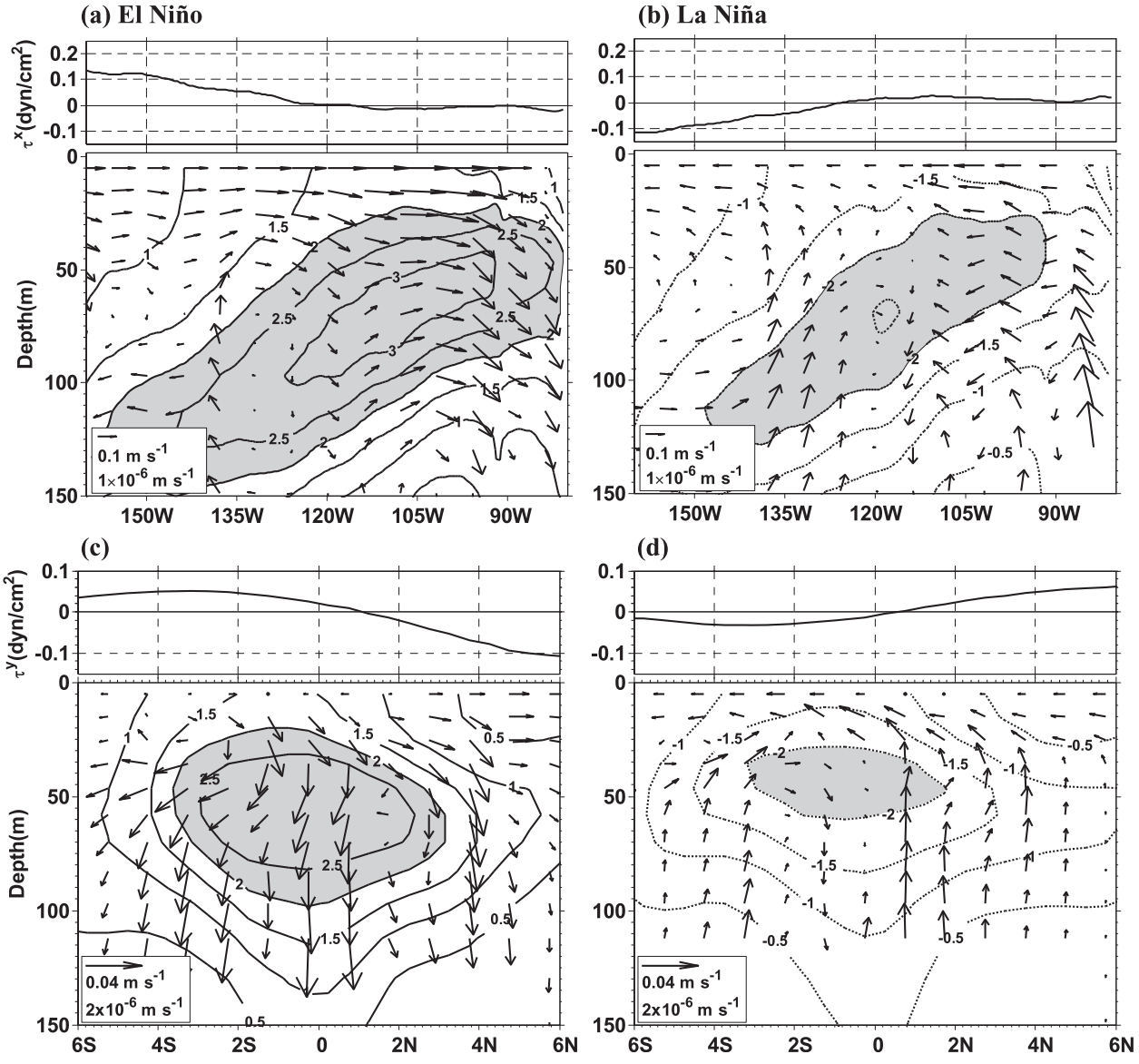

FIG. 7. (top) Composite mean zonal wind stress, temperature, and current anomalies along the equator (within ±2°) and (bottom) mean meridional wind stress, temperature, and current anomalies averaged in the eastern Pacific (110°–80°W) during developing phases for (left) El Niño and (right) La Niña from SODA 2.0.2. The temperature anomalies are shown as contours with an interval of 0.5°C, and absolute values >2.0°C are shaded.

where the meridional ocean current anomalies are northward (Fig. 7c). As a result, the meridional nonlinear advection term is positive ($-v'\partial T'/\partial y > 0$). In the La Niña composite, both the meridional temperature gradient and the meridional current anomalies are opposite to those in the El Niño composite. Hence, the meridional nonlinear advection terms are positive in the equatorial eastern Pacific during both the El Niño and La Niña events.

Because the temperature change in the subsurface (50–100 m) is larger than that in the surface (Fig. 7), the vertical gradient of the anomalous temperature is negative ($\partial T'/\partial z < 0$, where z is positive upward) for El Niño and positive for La Niña. During El Niño, there are strong downwelling anomalies east of 105°W (Fig. 7a). As a result, the vertical nonlinear advection tends to be negative there ($\partial T'/\partial z < 0$ and $w' < 0$; therefore, $-w'\partial T'/\partial z < 0$; Fig. 6c). During La Niña, the anomalous vertical current is upward; hence, the vertical nonlinear advection is also negative ($\partial T'/\partial z > 0$ and $w' > 0$; therefore, $-w'\partial T'/\partial z < 0$; Fig. 6d).

Although the nonlinear vertical advection is negative east of 110°W, it becomes positive over the maximum or

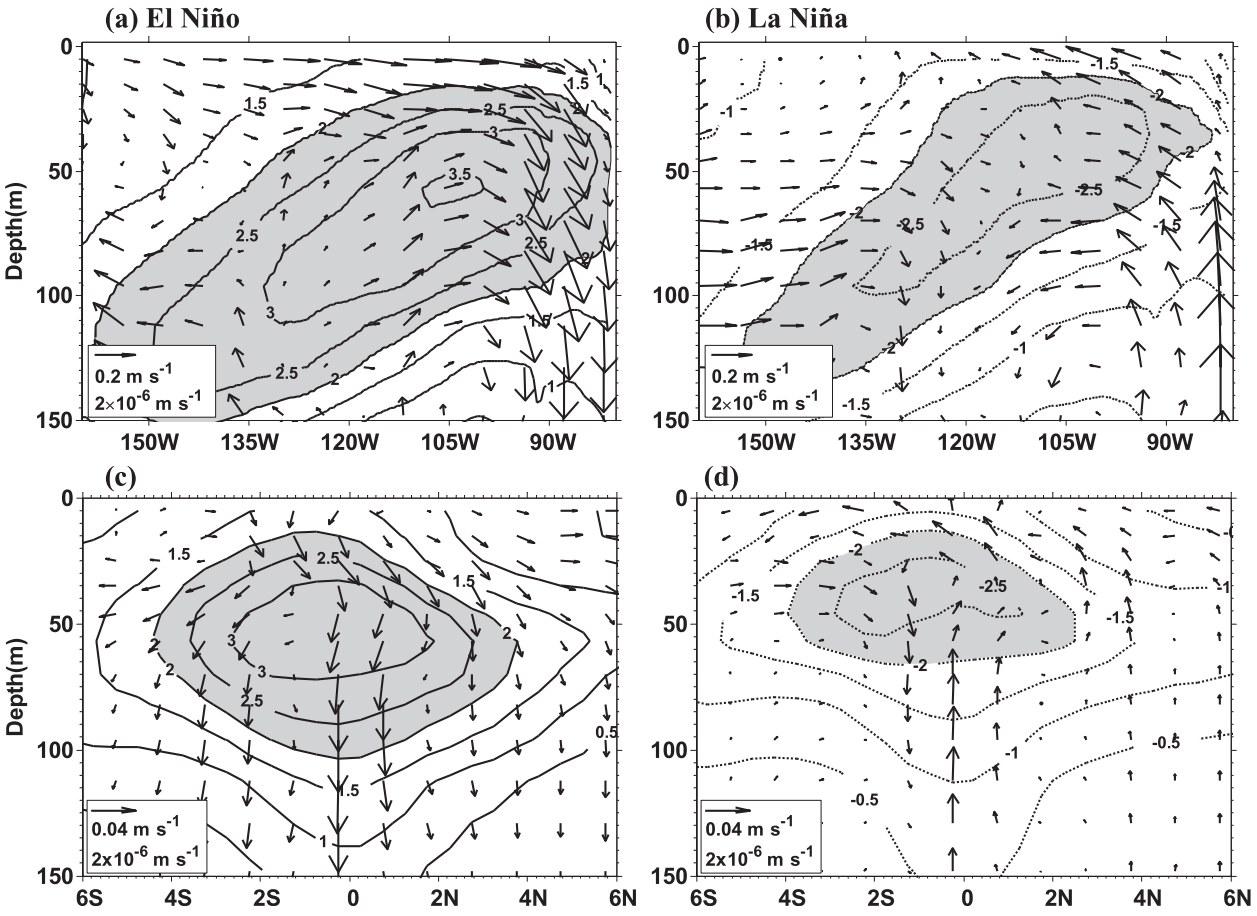

FIG. 8. (top) Composite mean temperature and zonal current anomalies along the equator (within ±2°) and (bottom) mean temperature and meridional current anomalies averaged in the eastern Pacific (110°–80°W) during developing phases for (left) El Niño and (right) La Niña events. The temperature anomalies are shown as contours with an interval of 0.5°C, and absolute values >2.0°C are shaded. The composite fields are the ensemble mean of SODA 1.4.2 and GODAS.

minimum SSTA center. For example, during the El Niño developing phase, there is anomalous upwelling at the base of the mixed layer at 110°W (Fig. 7a). As a result, the vertical nonlinear advection leads to the MLT warming, which is consistent with AJ04. However, the strongest amplitude asymmetry does not appear over the maximum SSTA center; rather, it appears in the far eastern equatorial Pacific (east of 110°W), where anomalous downwelling is pronounced (Fig. 7a). Hence, the vertical nonlinear advection tends to enhance (reduce) the SST warming around (east of) the maximum SSTA center. A similar vertical nonlinear advection feature occurs during the La Niña.

The contribution of the nonlinear advections to the ENSO amplitude asymmetry is further confirmed by the anomalous temperature and current fields from the ensemble of the SODA 1.4.2 and GODAS data (Fig. 8). The current anomalies in the far eastern Pacific show an opposite pattern between the warm and cold composites. In the El Niño composite, the zonal (meridional) current anomalies in the mixed layer are eastward (northward) and there is anomalous downwelling east of 110°W. As a result, the zonal and meridional nonlinear advections are positive, whereas the vertical nonlinear advection is negative. Similar results can be derived in the La Niña composite because the anomalous horizontal and vertical currents change their directions and the anomalous temperature changes its sign.

5. Cause of anomalous ocean circulation

A key question related to the positive skewness or the ENSO amplitude asymmetry is what causes the eastward (westward) current anomaly against the surface zonal wind stress anomaly in the far eastern Pacific during El Niño (La Niña). During El Niño, the enhanced convection near the maximum SSTA leads to a convergent surface wind stress pattern, with eastward (westward)

zonal wind stress anomaly in the western-central equatorial Pacific (east of 120°W) (Fig. 7a). The eastward ocean mixed-layer current is enhanced east of 120°W (Fig. 7a; Fig. 8a), with a direction against the westward wind stress in situ. This implies that the ocean current anomaly is not directly driven by the wind stress anomaly. The anomalous local vertical overturning circulation (with upward motion under the maximum SSTA center and downward motion to the east of 110°W) is, to a large extent, caused by the divergence of the eastward current anomalies. Therefore, a physical interpretation is required for understanding the cause of the anomalous mixed-layer ocean currents.

To investigate the mechanisms for generating the current anomalies, wind-induced Ekman currents and geostrophic currents are diagnosed in an equatorial β-plane framework. The linear reduced-gravity model in an equatorial β plane forced by the surface wind stress has been used to study current anomalies associated with ENSO (e.g., Hirst 1986; Wang and Weisberg 1994). The anomalous zonal and meridional geostrophic currents may be written as

$$u_g = -\frac{g'}{\beta}\frac{\partial^2 h}{\partial y^2} \quad \text{and} \tag{2}$$

$$v_g = \frac{g'}{\beta}\frac{\partial^2 h}{\partial x \partial y}, \tag{3}$$

where $g' = 0.026$ m s^{-2} is the reduced gravity, β is the planetary vorticity gradient, and h is the anomalous thermocline depth. Here, the thermocline depth is represented by the depth of 18°C isotherm. The anomalous Ekman currents are calculated based on Chang and Philander (1994):

$$u_e = \frac{1}{\rho H_1}\frac{r_s \tau^x + \beta y \tau^y}{r_s^2 + (\beta y)^2} \quad \text{and} \tag{4}$$

$$v_e = \frac{1}{\rho H_1}\frac{r_s \tau^y - \beta y \tau^x}{r_s^2 + (\beta y)^2}, \tag{5}$$

where ρ is the density of seawater; H_1 is the mean mixed-layer depth; τ^x and τ^y are the zonal and meridional wind stress anomalies, respectively; and $r_s = (1/2)$ day^{-1} is the dissipation rate.

The calculated zonal geostrophic and Ekman current anomalies are shown in Fig. 9. Note that the zonal current anomalies in the far eastern equatorial Pacific are primarily contributed by the geostrophic current, whereas the wind-induced Ekman current is one order of magnitude smaller and its direction is opposite to that of the geostrophic current. This feature appears in both El Niño and La Niña events (Figs. 9a,b).

The anomalous geostrophic current in the eastern equatorial Pacific is closely related to the variation of the thermocline depth in situ. During the onset and development phases of El Niño, westerly wind anomalies in the western equatorial Pacific may produce downwelling Kelvin waves to warm the equatorial central and eastern Pacific (e.g., Weisberg and Wang 1997a,b; Wang and Weisberg 2000). The composite mean temperature fields show a deepening of the thermocline depth with a magnitude of about 30 m in the eastern Pacific. It is the maximum thermocline depth anomaly in the eastern equatorial Pacific that leads to a positive geostrophic current anomaly in situ. The zonal current anomaly that is generated further induces a local vertical overturning circulation, with anomalous upwelling around the maximum SSTA center (~110°W) and anomalous downwelling to its east (Figs. 7a, 8a). A reversed local overturning circulation appears during La Niña (Figs. 7b, 8b).

In contrast to the dominant geostrophic zonal current, the meridional current anomaly in EP110 arises primarily from the anomalous Ekman current, whereas the magnitude of the meridional geostrophic current anomaly is much smaller (Fig. 10). It is worth mentioning that, although the maximum (minimum) SSTA during El Niño (La Niña) appears south of the equator, the maximum convergence (divergence) of the surface meridional wind is located north of the equator (Figs. 7c,d). This is crucial for forcing a northward (southward) Ekman current anomaly during El Niño (La Niña), which leads to a positive MLT tendency for both warm and cold episodes. The northward shift of the anomalous surface atmospheric convergence (and convection) is primarily caused by the equatorial asymmetry of the mean SST, because the anomalous convection is determined by both the SSTA and mean SST (Zebiak and Cane 1987; Li et al. 2003). Although the SSTA is relatively weak north of the equator, the mean SST is much higher there. As a result, anomalous atmospheric convection and surface wind convergence appear to the north of the equator.

The relative contribution of the geostrophic and Ekman currents to the ocean circulation changes can be further validated from the results calculated based on SODA 1.4.2 and GODAS (Figs. 9c,d, 10). Thus, the zonal current is primarily attributed to the anomalous geostrophic current, whereas the meridional circulation is dominated by the anomalous Ekman current.

6. Conclusions and discussion

The amplitude asymmetry of the SSTA between El Niño and La Niña is investigated by diagnosing a mixed-layer heat budget during the developing phases of ENSO. The budget analysis indicates that the nonlinear

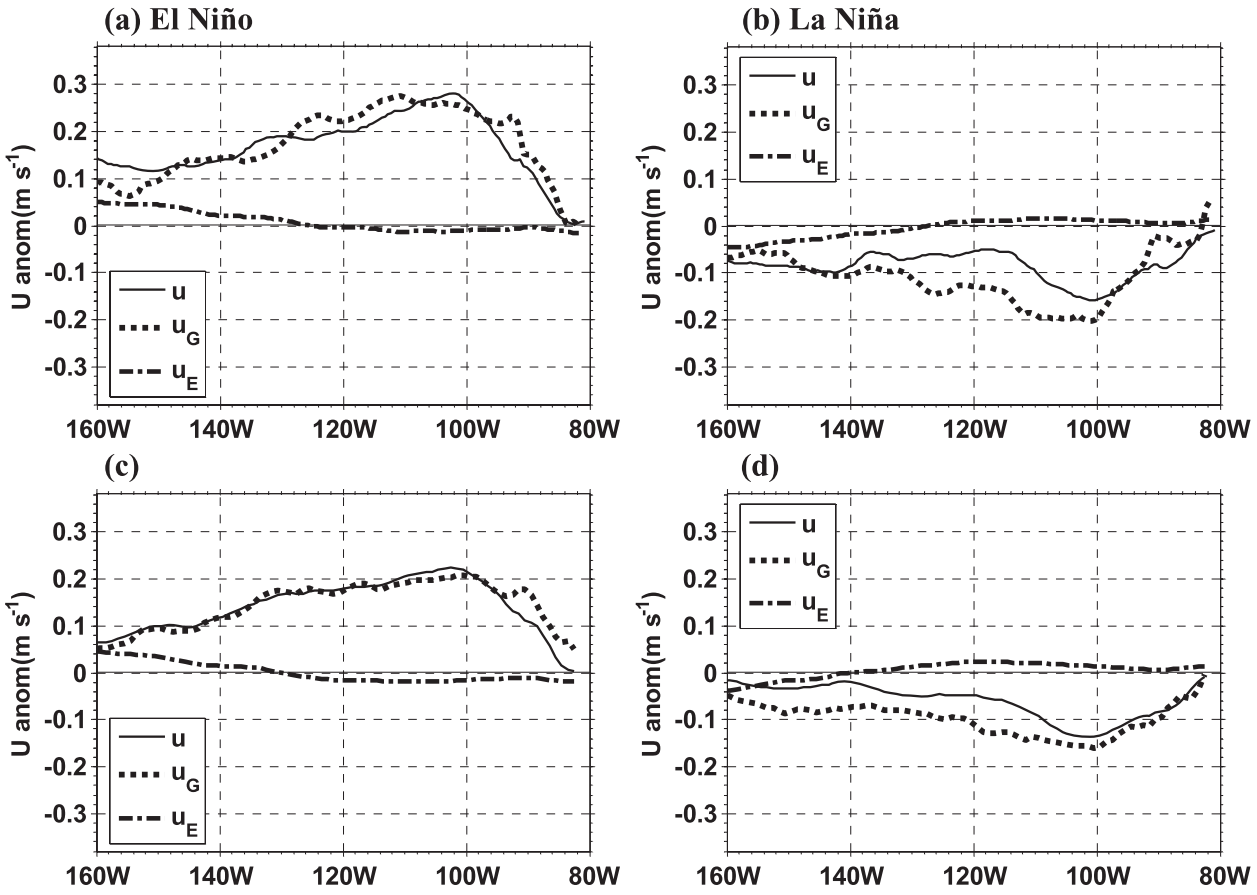

FIG. 9. Anomalies of zonal currents from the assimilated ocean data (solid line), geostrophic currents (dotted line), and Ekman currents (dotted–dashed line) along the equator (within ±2°) during developing phases for (left) El Niño and (right) La Niña based on (top) SODA 2.0.2 and (bottom) the ensemble mean of SODA 1.4.2 and GODAS.

zonal and meridional temperature advections are essential to cause the positive skewness in the equatorial eastern Pacific. The nonlinear vertical advection, on the other hand, favors the negative skewness because of the reduction (enhancement) of the upwelling of anomalous warm (cold) water from the subsurface layer to the mixed layer during El Niño (La Niña) events.

The cause of the positive skewness by the nonlinear zonal advection is attributed to anomalous geostrophic currents that are against the zonal wind stress anomaly. During El Niño (La Niña), the anomalous wind stress in response to the warm (cold) SSTA leads to the deepening (shoaling) of the thermocline depth, which causes eastward (westward) geostrophic current anomalies in the eastern equatorial Pacific. This leads to warm nonlinear zonal advections for both El Niño and La Niña episodes. The nonlinear meridional advection by anomalous Ekman currents also contributes to the positive skewness. The eastward (westward) zonal currents during El Niño (La Niña) result in the anomalous downwelling (upwelling) in the far eastern equatorial Pacific, which leads to cold vertical nonlinear advections in both warm and cold episodes.

Different from the ENSO developing phase, the nonlinear vertical advection during its mature–decaying phase is positive for both El Niño and La Niña, which is consistent with AJ04. This can be seen from the anomalous temperature and current fields during the mature–decaying phase (Fig. 11). Here, the mature–decaying periods for El Niño are as follows: October 1965–January 1966, October 1972–March 1973, November 1976–January 1978, February 1983–November 1983, July–December 1987, January–September 1992, and December 1997–September 1998. For La Niña, the mature–decaying periods are as follows: November–December 1964, October 1967–April 1968, December 1970–August 1971, November 1973–February 1974, May 1985–January 1986, October 1988–June 1989, and November 1999–March 2000. Although the vertical temperature gradient anomalies remain similar, the anomalous currents during the mature–decaying phase show a quite different pattern from the developing phase. In the far eastern

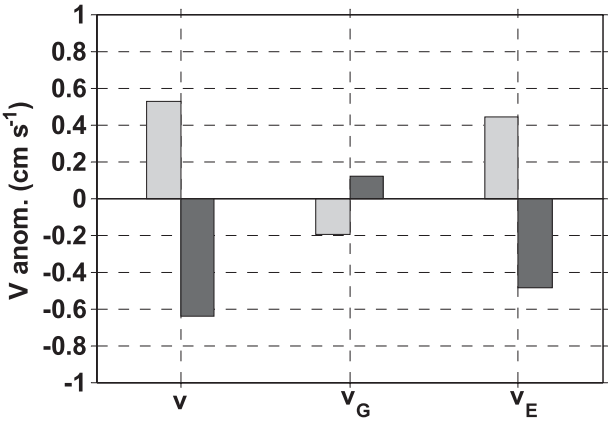

FIG. 10. Anomalies of meridional currents from ocean assimilation products (left bars), geostrophic meridional currents (middle bars), and Ekman meridional currents (right bars) averaged in the far eastern equatorial Pacific (2°S–2°N, 110°–80°W). Gray and black bars represent composite results of El Niño and La Niña events, respectively. The composite is based on the ensemble mean of SODA 2.0.2, SODA 1.4.2, and GODAS.

equatorial Pacific, anomalous upwelling (downwelling) appears east of about 120°W during the mature–decaying periods of El Niño (La Niña). This leads to positive vertical nonlinear temperature advection in the mature–decaying phase for both El Niño and La Niña. Thus, the nonlinear vertical temperature advection makes an opposite contribution during the ENSO developing and decaying phases. The positive vertical nonlinear warming in the mature–decaying phase, however, cannot contribute to the SSTA amplitude asymmetry because the actual temperature change will occur after the mature phase, when the SSTA has already reached its maximum or minimum.

It is important to note that, although all three products (SODA 2.0.2, SODA 1.4.2, and GODAS) indicate a positive horizontal nonlinear advection and a negative vertical nonlinear advection during the ENSO developing phase, the result from the older dataset ODAS (Ji and Smith 1995; Ji et al. 1995; Behringer et al. 1998) is different. The ODAS has a Pacific basin domain, with a horizontal resolution of 1.5° longitude by 1° latitude and a vertical resolution of 10 m in the upper 100-m depth. It covers the period of 1980–99. A comparison of the anomalous vertical velocity, vertical temperature difference, and nonlinear vertical temperature advection patterns between ODAS and GODAS during the 1997/98 El Niño episode is shown in Fig. 12. In the ODAS data, there is no direct output of the vertical velocity field and the vertical velocity is calculated from the horizontal currents by using the continuity equation. The vertical velocity pattern calculated from ODAS (Fig. 12a) resembles that in AJ04. Both the GODAS and ODAS show that the subsurface temperature anomalies are larger than the surface anomalies during the developing period of El Niño. Thus, the vertical temperature difference is negative prior to December 1997. The remarkable difference between ODAS and GODAS lies in the anomalous vertical velocity field. It is negative in GODAS (Fig. 12d) but positive in ODAS (Fig. 12a) in the far eastern equatorial Pacific (east of 120°W) during January–December 1997. As a result, the anomalous vertical nonlinear temperature advection in the far eastern Pacific is different in the two datasets, being positive in ODAS (Fig. 12c) but negative in GODAS (Fig. 12f). A significant difference in the vertical velocity and vertical nonlinear advection fields between ODAS

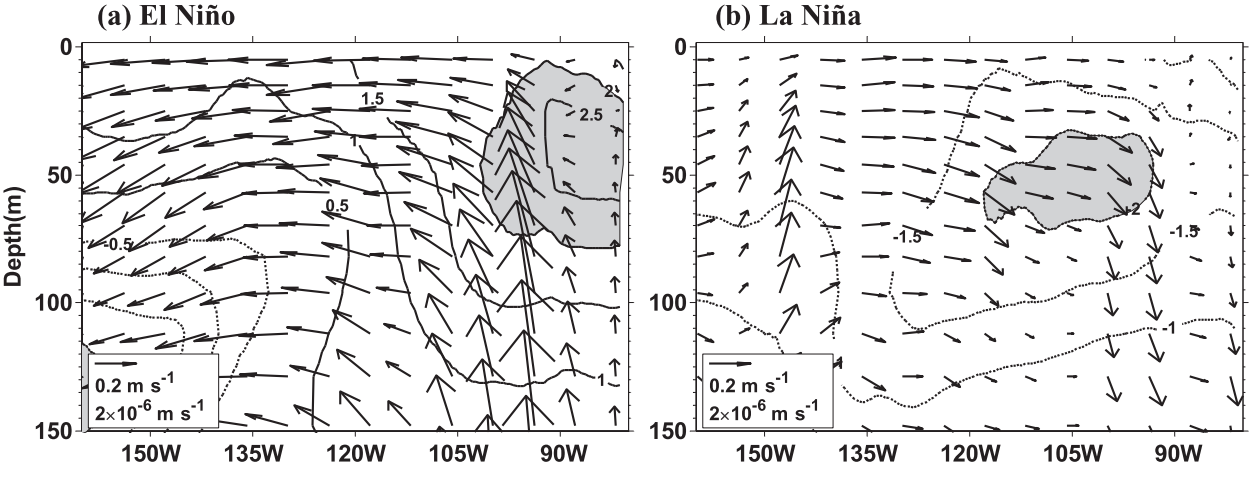

FIG. 11. Composite temperature and current anomalies along the equator (within ±2°) during the mature–decaying phase of (a) El Niño and (b) La Niña. The temperature anomalies are shown as contours with an interval of 0.5°C, and the absolute values >2.0°C are shaded. The composite fields are the ensemble mean of SODA 2.0.2, SODA 1.4.2, and GODAS.

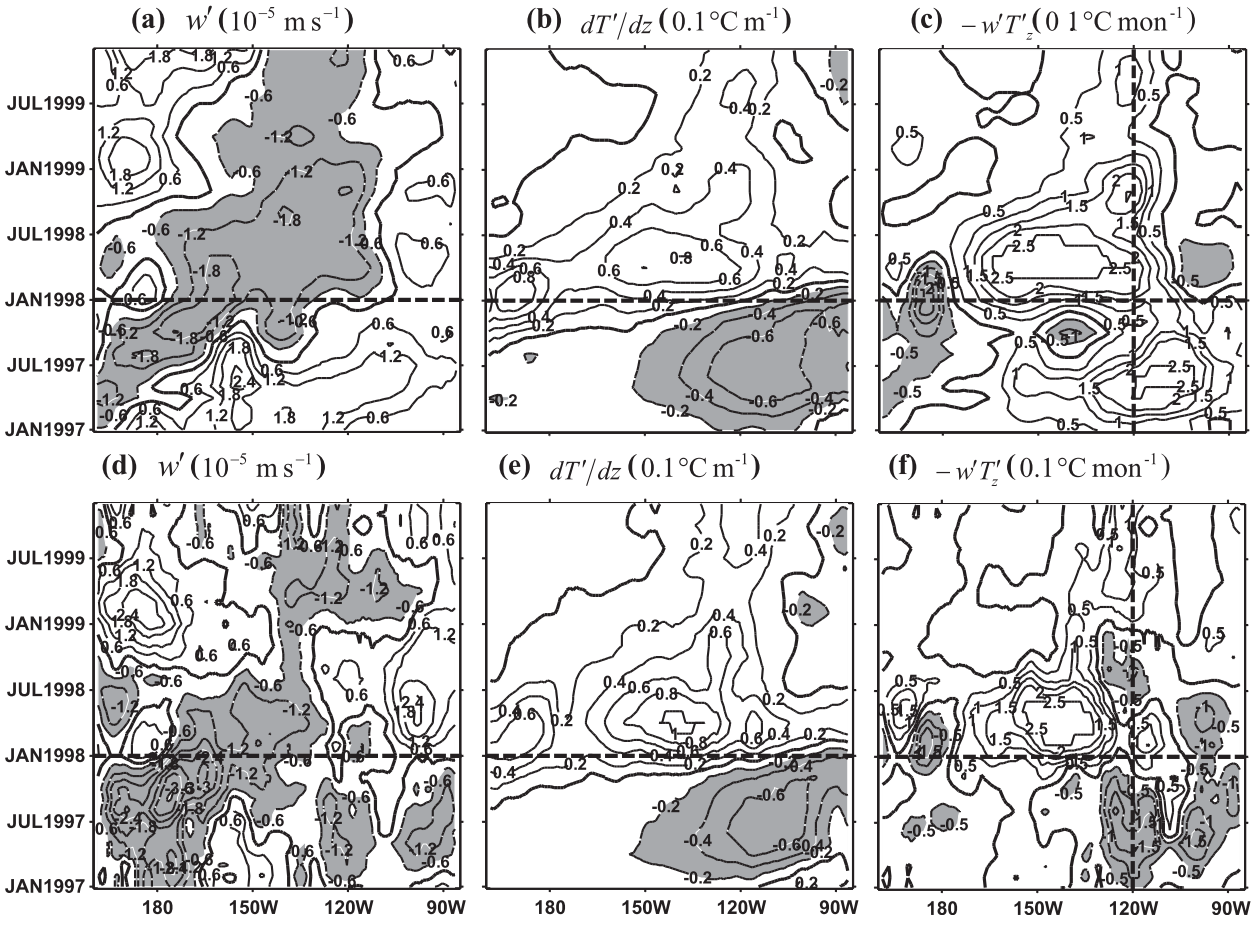

FIG. 12. Longitude–time section along the equator (averaged over 0.5°S–0.5°N) of anomalous upwelling velocity (10^{-5} m s^{-1}), vertical temperature difference (0.1°C m^{-1}), and nonlinear vertical advection (0.1°C month^{-1}) during the 1997/98 El Niño episode derived from (top) ODAS and (bottom) GODAS. The thick black line represents the zero line, and large negative values are shaded.

and GODAS is also found during the developing phase of the 1982/83 El Niño.

The vertical velocity difference also appears between SODA 2.0.2 and SODA beta 7 version products. In the SODA beta 7 version (Carton et al. 2000), MOM2 is forced by NCEP surface wind stress and heat fluxes during 1950–2001. Although the anomalous temperatures are similar to those in SODA 2.0.2, the SODA beta version shows a quite different vertical current anomaly field in the far eastern Pacific. For example, anomalous upwelling in the beta version appears east of 120°W prior to December 1997, which is opposite of that from SODA 2.0.2 (Fig. 13). This anomalous upwelling in the far eastern Pacific in the beta version would cause a positive vertical nonlinear heating to enhance El Niño, as emphasized in AJ04. The above comparison indicates that caution is needed in diagnosing the ocean heat budget, in particular the vertical temperature advection, and it is necessity to use multiple ocean assimilation data products to validate the analysis results.

The ocean current fields derived from SODA 2.0.2 and GODAS may be verified by independent ocean observations such as the Ocean Surface Currents Analysis–Real Time (OSCAR; Lagerloef et al. 1999). OSCAR currents are designed to represent the average over a 30-m-thick surface layer. The OSCAR dataset is routinely updated every week and covers the period from October 1992 to the present. It provides reasonably accurate time means of horizontal currents at a period of 40 days or longer and a wavelength of 8° or greater (Johnson et al. 2007). Figure 14 shows the time series of vertical velocity anomalies at the depth of 30 m from OSCAR (calculated from the horizontal current fields based on the continuity equation), along with those from SODA 2.0.2 and beta 7 during the period of 1993–2000. It is obvious that the time series of SODA 2.0.2 is much closer to that of OSCAR. Although there is a significant positive correlation between the two, the correlation between OSCAR and SODA beta 7 is near zero. Prior to the mature phase of the 1997/98 El Niño, negative

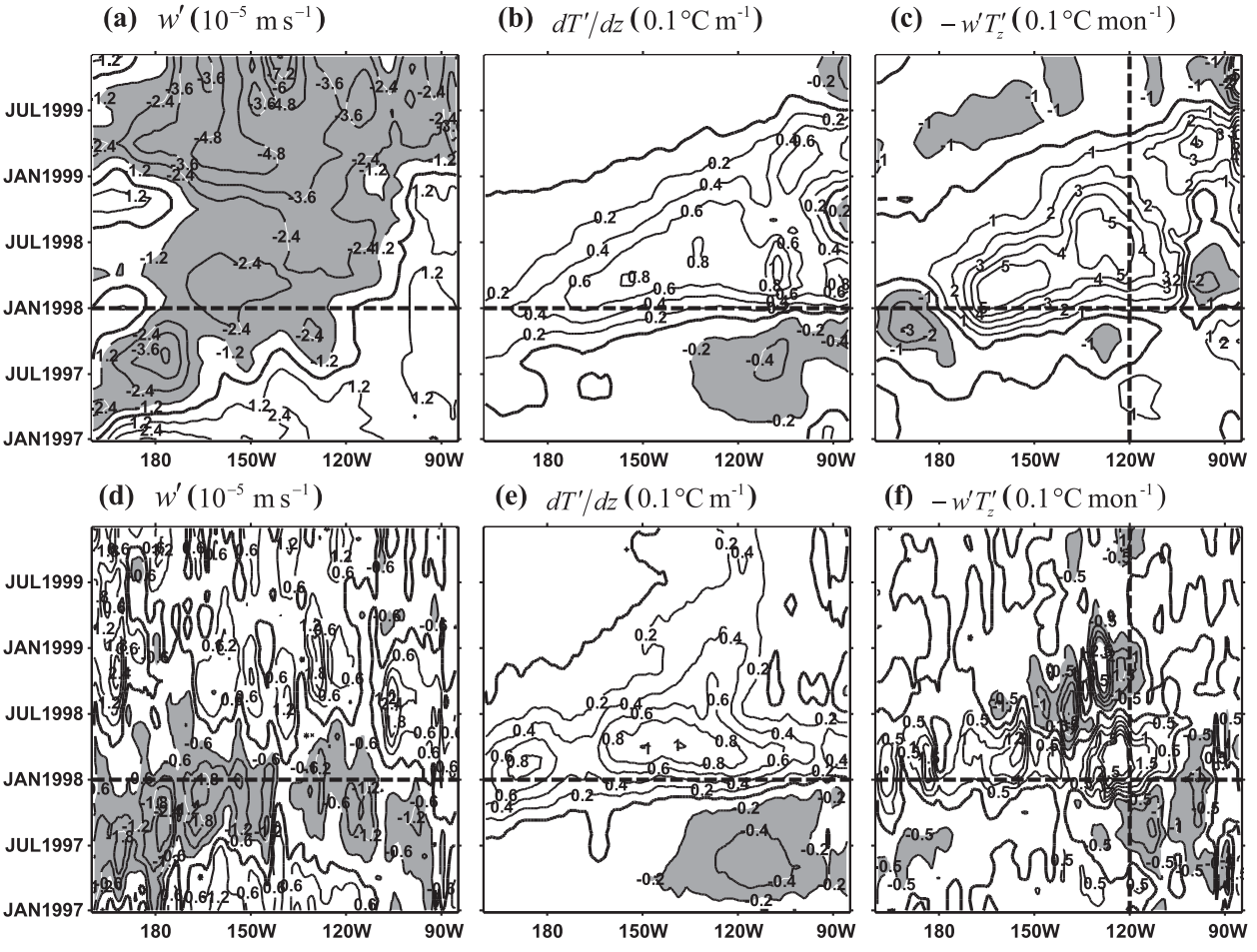

FIG. 13. As in Fig. 12, but for SODA (top) beta 7 and (bottom) 2.0.2.

vertical velocity anomalies appeared in the far eastern equatorial Pacific in OSCAR, which is consistent with those derived from SODA 2.0.2 (and GODAS) but remarkably different from the SODA beta 7 (and ODAS; Fig. 14). The independent observational data further validate the conclusions derived from the current study.

Acknowledgments. This work was supported by the National Basic Research Program of China (2007CB816005), NSFC (No. 40706003, 40921003), and the International S&T Cooperation Project of the Ministry of Science and Technology of China (No. 2009DFA21430). TL was supported by CMA and NSFC Grants

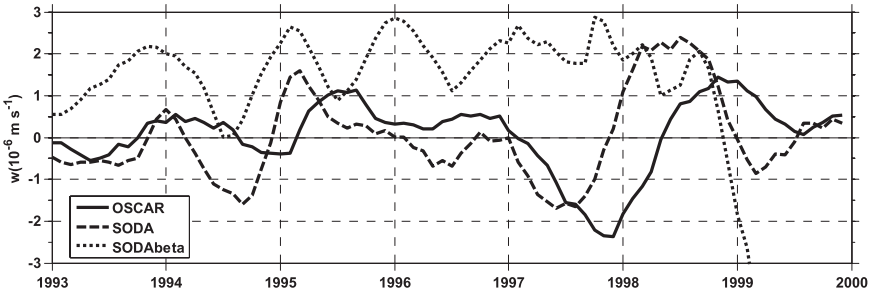

FIG. 14. The time series of vertical velocity anomalies at a depth of 30 m in EP110 (5°N–5°S, 110°–80°W) from OSCAR (solid line), SODA 2.0.2 (dashed line), and SODA beta 7 (dotted line) products. The time series has been smoothed with a 7-month running mean.

40628006/40675054; ONR Grants N000140710145 and N000140810256; and the International Pacific Research Center, which is sponsored by the Japan Agency for Marine-Earth Science and Technology (JAMSTEC), NASA (NNX07AG53G), and NOAA (NA17RJ1230).

REFERENCES

An, S. I., and F. F. Jin, 2004: Nonlinearity and asymmetry of ENSO. *J. Climate,* **17,** 2399–2412.

Battisti, D. S., and A. C. Hirst, 1989: Interannual variability in a tropical atmosphere–ocean model: Influence of the basic state, ocean geometry and nonlinearity. *J. Atmos. Sci.,* **46,** 1687–1712.

Behringer, D. W., M. Ji, and A. Leetmaa, 1998: An improved coupled model for ENSO prediction and implications for ocean initialization. Part I: The ocean data assimilation system. *Mon. Wea. Rev.,* **126,** 1013–1021.

Burgers, G., and D. B. Stephenson, 1999: The ''normality'' of El Niño. *Geophys. Res. Lett.,* **26,** 1027–1030.

Cane, M. A., and S. E. Zebiak, 1985: A theory of El Niño and the Southern Oscillation. *Science,* **228,** 1084–1087.

Carton, J. A., and B. S. Giese, 2008: A reanalysis of ocean climate using Simple Ocean Data Assimilation (SODA). *Mon. Wea. Rev.,* **136,** 2999–3017.

——, G. Chepurin, X. Cao, and B. Giese, 2000: A simple ocean data assimilation analysis of the global upper ocean 1950–95. Part I: Methodology. *J. Phys. Oceanogr.,* **30,** 294–309.

Chang, P., and S. G. Philander, 1994: A coupled ocean–atmosphere instability of relevance to the seasonal cycle. *J. Atmos. Sci.,* **51,** 3627–3648.

Dukowicz, J., and R. D. Smith, 1994: Implicit free-surface method for the Bryan-Cox-Semtner ocean model. *J. Geophys. Res.,* **99,** 7991–8014.

Hirst, A. C., 1986: Unstable and damped equatorial modes in simple coupled ocean-atmosphere models. *J. Atmos. Sci.,* **43,** 606–632.

Hoerling, M. P., A. Kumar, and M. Zhong, 1997: El Niño, La Niña, and the nonlinearity of their teleconnections. *J. Climate,* **10,** 1769–1786.

Hong, C.-C., T. Li, L. Ho, and J.-S. Kug, 2008a: Asymmetry of the Indian Ocean dipole. Part I: Observational analysis. *J. Climate,* **21,** 4834–4848.

——, ——, and J.-J. Luo, 2008b: Asymmetry of the Indian Ocean dipole. Part II: Model diagnosis. *J. Climate,* **21,** 4849–4858.

Ji, M., and T. M. Smith, 1995: Ocean model response to temperature data and varying surface wind stress: Intercomparisons and implications for climate forecast. *Mon. Wea. Rev.,* **123,** 1811–1821.

——, A. Leetmaa, and J. Derber, 1995: An ocean analysis system for seasonal to interannual climate studies. *Mon. Wea. Rev.,* **123,** 460–481.

Jin, F.-F., 1997: An equatorial ocean recharge paradigm for ENSO. Part I: Conceptual model. *J. Atmos. Sci.,* **54,** 811–829.

——, S.-I. An, A. Timmermann, and J. Zhao, 2003: Strong El Niño events and nonlinear dynamical heating. *Geophys. Res. Lett.,* **30,** 1120, doi:10.1029/2002GL016356.

Johnson, E. S., F. Bonjean, G. S. E. Lagerloef, J. T. Gunn, and G. T. Mitchum, 2007: Validation and error analysis of OSCAR sea surface currents. *J. Atmos. Oceanic Technol.,* **24,** 688–701.

Kang, I.-S., and J.-S. Kug, 2002: El Niño and La Niña sea surface temperature anomalies: Asymmetry characteristics associated with their wind stress anomalies. *J. Geophys. Res.,* **107,** 4372, doi:10.1029/2001JD000393.

Lagerloef, G. S. E., G. T. Mitchum, R. B. Lukas, and P. P. Niiler, 1999: Tropical Pacific near-surface currents estimated from altimeter, wind, and drifter data. *J. Geophys. Res.,* **104,** 23 313–23 326.

Li, T., 1997: Phase transition of the El Niño–Southern Oscillation: A stationary SST mode. *J. Atmos. Sci.,* **54,** 2872–2887.

——, Y. S. Zhang, E. Lu, and D. Wang, 2002: Relative role of dynamic and thermodynamic processes in the development of the Indian Ocean dipole. *Geophys. Res. Lett.,* **29,** 2110–2113.

——, B. Wang, C.-P. Chang, and Y. Zhang, 2003: A theory for the Indian Ocean dipole–zonal mode. *J. Atmos. Sci.,* **60,** 2119–2135.

Philander, S. G. H., 1990: *El Niño, La Niña, and the Southern Oscillation*. Academic Press, 293 pp.

Picaut, J., F. Masia, and Y. du Penhoat, 1997: An advective–reflective conceptual model for the oscillatory nature of the ENSO. *Science,* **277,** 663–666.

Rasmusson, E. M., and T. H. Carpenter, 1982: Variations in tropical sea surface temperature and surface wind fields associated with the Southern Oscillation/El Niño. *Mon. Wea. Rev.,* **110,** 354–384.

Saha, S., and Coauthors, 2006: The NCEP Climate Forecast System. *J. Climate,* **19,** 3483–3517.

Suarez, M. J., and P. S. Schopf, 1988: A delayed action oscillator for ENSO. *J. Atmos. Sci.,* **45,** 3283–3287.

Vialard, J., C. Menkes, J.-P. Boulanger, P. Delecluse, E. Guilyardi, M. J. McPhaden, and G. Madec, 2001: A model study of oceanic mechanisms affecting equatorial Pacific sea surface temperature during the 1997–98 El Niño. *J. Phys. Oceanogr.,* **31,** 1649–1675.

Wang, C., and R. H. Weisberg, 1994: On the ''slow mode'' mechanism in ENSO-related coupled ocean–atmosphere models. *J. Climate,* **7,** 1657–1667.

——, and ——, 2000: The 1997–98 El Niño evolution relative to previous El Niño events. *J. Climate,* **13,** 488–501.

Weisberg, R. H., and C. Wang, 1997a: A western Pacific oscillator paradigm for the El Niño-Southern Oscillation. *Geophys. Res. Lett.,* **24,** 779–782.

——, and ——, 1997b: Slow variability in the equatorial west-central Pacific in relation to ENSO. *J. Climate,* **10,** 1998–2017.

White, H. G., 1980: Skewness, kurtosis and extreme values of Northern Hemisphere geopotential heights. *Mon. Wea. Rev.,* **108,** 1446–1455.

Zebiak, S. E., and M. A. Cane, 1987: A model ENSO. *Mon. Wea. Rev.,* **115,** 2262–2278.

Zhang, R., and J. Chao, 1993a: Unstable tropical air-sea interaction waves and their physical mechanisms. *Adv. Atmos. Sci.,* **10,** 61–70.

——, and ——, 1993b: Mechanisms of interannual variations in a simple air-sea coupled model in the tropics. *Climate Variability,* Y. Duzheng at el., Eds., China Meteorological Press, 236–244.

CORRIGENDUM

JINGZHI SU,* RENHE ZHANG,+ TIM LI,# XINYAO RONG,+ J.-S. KUG,@ AND CHI-CHERNG HONG&

* *Chinese Academy of Meteorological Sciences, and Nansen-Zhu International Research Centre, Institute of Atmospheric Physics, Chinese Academy of Sciences, Beijing, China*
+ *Chinese Academy of Meteorological Sciences, Beijing, China*
# *Department of Meteorology, University of Hawaii at Manoa, Honolulu, Hawaii*
@ *Korea Ocean Research and Development Institute, Ansan, South Korea*
& *Department of Science Education, Taipei Municipal University of Education, Taipei*

There was an error in the affiliations list of the coauthors for Su et al. (2010). For coauthor C.-C. Hong, the correct affiliation should be Department of Science Education, Taipei Municipal University of Education, Taipei; and for coauthor Tim Li, the correct affiliation should be Department of Meteorology, University of Hawaii at Manoa, Honolulu, Hawaii. The full list of authors and their affiliations is given correctly above. In addition, in the acknowledgments, the following addition is made: J.-S. Kug is supported by the Korea Meteorological Administration Research and Development Program under Grant CATER 2006-4202.

The staff of the *Journal of Climate* regrets any inconvenience this error may have caused.

REFERENCE

Su, J., R. Zhang, T. Li, X. Rong, J.-S. Kug, and C.-C. Hong, 2010: Causes of the El Niño and La Niña amplitude asymmetry in the equatorial eastern Pacific. *J. Climate,* **23,** 605–617.

DOI: 10.1175/2010JCLI3778.1